Distinct roles of the last transmembrane domain in controlling *Arabidopsis* K^+ channel activity

Pawel Gajdanowicz[1], Carlos Garcia-Mata[2,3], Wendy Gonzalez[1,4], Samuel Elías Morales-Navarro[4], Tripti Sharma[1,5], Fernando Danilo González-Nilo[4], Jan Gutowicz[6], Bernd Mueller-Roeber[5,7], Michael R. Blatt[2] and Ingo Dreyer[1]

[1]Universität Potsdam, Institut für Biochemie und Biologie, Heisenberg-Gruppe Biophysik und Molekulare Pflanzenbiologie, 14476 Potsdam/Golm, Germany; [2]Laboratory of Plant Physiology and Biophysics, IBLS Plant Sciences, Bower Building, University of Glasgow, Glasgow G12 8QQ, UK; [3]Laboratorio de Fisiologia Molecular e Integrativa, Institutos de Investigaciones Biologicas, Universidad Nacional de Mar del Plata, 7600 Mar del Plata, Buenos Aires, Argentina; [4]Centro de Bioinformática y Simulación Molecular, Universidad de Talca, Casilla 721, Talca, Chile; [5]Max-Planck Institute of Molecular Plant Physiology, 14476 Potsdam/Golm, Germany; [6]Department of Physical Chemistry of Microorganisms, Institute of Genetics and Microbiology, University of Wrocław, 51148 Wrocław, Poland; [7]Universität Potsdam, Institut für Biochemie und Biologie, Abteilung Molekularbiologie, 14476 Potsdam/Golm, Germany

Author for correspondence:
Ingo Dreyer
Tel: +49 331 977 2809
Fax: +49 331 977 2512
Email: dreyer@uni-potsdam.de

Received: *23 October 2008*
Accepted: *29 November 2008*

New Phytologist (2009)
doi: 10.1111/j.1469-8137.2008.02749.x

Key words: *Arabidopsis*, channel protein structure, channel protein–cation interaction, gating, inward rectifier, K^+ channel, K^+-dependent, outward rectifier.

Summary

- The family of voltage-gated potassium channels in plants presumably evolved from a common ancestor and includes both inward-rectifying (K_{in}) channels that allow plant cells to accumulate K^+ and outward-rectifying (K_{out}) channels that mediate K^+ efflux. Despite their close structural similarities, the activity of K_{in} channels is largely independent of K^+ and depends only on the transmembrane voltage, whereas that of K_{out} channels responds to the membrane voltage and the prevailing extracellular K^+ concentration. Gating of potassium channels is achieved by structural rearrangements within the last transmembrane domain (S6).
- Here we investigated the functional equivalence of the S6 helices of the K_{in} channel KAT1 and the K_{out} channel SKOR by domain-swapping and site-directed mutagenesis. Channel mutants and chimeras were analyzed after expression in *Xenopus* oocytes.
- We identified two discrete regions that influence gating differently in both channels, demonstrating a lack of functional complementarity between KAT1 and SKOR. Our findings are supported by molecular models of KAT1 and SKOR in the open and closed states.
- The role of the S6 segment in gating evolved differently during specialization of the two channel subclasses, posing an obstacle for the transfer of the K^+-sensor from K_{out} to K_{in} channels.

Introduction

Potassium channels of the plant plasma membrane comprise a major set of pathways for K^+ ion flux, contributing to maintenance of cellular hydrostatic (turgor) pressure as well as to growth and responses to biotic and abiotic stresses. Different subsets of K^+ channels with distinct biophysical and regulatory characteristics ensure an appropriate balance of K^+ ion flux. They enable plant cells to accommodate changes in the extracellular ionic environment and in the homeostatic needs of the cell, including diverse roles in charge balance for phloem (un)loading, K^+ uptake at the root–soil interface, and K^+ uptake into, and loss from stomatal guard cells at the leaf epidermis (Véry & Sentenac, 2003; Dreyer *et al.*, 2004a; Blatt *et al.*, 2007). These unique demands on K^+ transport across plant membranes has engendered a number of features associated with the gating of several of these K^+ channels, rendering their study unusually rich with information bearing on the functional versatility of this class of integral membrane proteins.

In no instance has this proved more true than for the family of voltage-gated (Kv) K^+ channels that share close structural similarities with the *Drosophila Shaker* K^+ channel. Voltage-gated plant K^+ channels presumably have evolved from a common ancestor because they comprise a common framework of six

transmembrane domains, designated S1–S6, with the pore region between transmembrane segments S5 and S6 that forms the major constriction and lining of the pore. Structurally, these K^+ channels are relatively homogeneous. In their central transmembrane cores, which comprise the rectification properties of the channels (Cao *et al.*, 1995; Dreyer *et al.*, 2004b; Poree *et al.*, 2005), they share identities of 40% or higher. However, the same channels show an amazing diversity, segregating between at least three distinct subfamilies based on their functional characteristics (Pilot *et al.*, 2003; Dreyer *et al.*, 2004a). Among them are inward-rectifying channels (K_{in} channels) and outward-rectifying channels (K_{out} channels). K_{in} channels share common features of activation upon membrane hyperpolarization and a largely static frame of voltages for the transition between open and closed states. As a consequence, they function as potassium uptake channels, allowing plant cells the accumulation of K^+ from the soil or the extracellular environment. K_{out} channels, by contrast, exhibit profound activation on membrane depolarization. These channels also activate over a dynamic range of voltages that depend on the K^+ concentration prevailing outside the cell, $[K^+]_o$ (Gaymard *et al.*, 1998; Ache *et al.*, 2000; Hosy *et al.*, 2003; Johansson *et al.*, 2006). Intriguingly, this K^+ sensitivity clearly differs from that of analogous mammalian K^+ channels (Pardo *et al.*, 1992; Sanguinetti *et al.*, 1995). Generally, the mammalian channels are activated with increasing external potassium concentration and deactivated when the K^+ concentration decreases, but their gating remains static within a fixed range of membrane voltages. By contrast, K_{out} channels open only at membrane voltages positive of the equilibrium potential for potassium, E_K, shifting their range of activity to more positive voltages as the external K^+ concentration increases (Blatt & Gradmann, 1997). This ability to sense the external K^+ concentration carries profound biological significance, because it ensures that the channels open only when the driving force for net K^+ flux is directed outwards, even when the extracellular K^+ varies over concentrations from 10 nM to 100 mM. Plants take advantage of this gating dynamic in K_{out} channels, for example in driving K^+ flux for stomatal closure (Blatt & Gradmann, 1997; Hosy *et al.*, 2003) and xylem loading (Gaymard *et al.*, 1998).

Elements of the molecular mechanism behind this sensitivity to extracellular K^+ were recently detailed for the K_{out} channel SKOR (Johansson *et al.*, 2006). In this channel, K^+ sensing is achieved by a mechanism that effectively 'counts' the time-averaged number of K^+ ions in the mouth of the pore when the channel is closed (i.e. when the pore is accessible only from the extracellular membrane surface). SKOR incorporates an 'S6 gating domain', including the key residues D-M-I, within the last transmembrane segment that opposes and interacts with the base of the pore helix, transmitting information about pore occupancy to the channel gate. Altering this interaction through residue exchange – either in the S6 gating domain or at the base of the pore helix – affects the K^+ sensitivity as well as the voltage-dependence of SKOR gating and, in the extreme, also renders the channel nonrectifying (Johansson *et al.*, 2006).

These results raised the challenging question of whether the S6 regions of K_{in} and K_{out} channels diverge in their function. Therefore, we have investigated the reciprocal functionality of the S6 helix between KAT1 and SKOR. It is shown that these regions are important for channel gating, but their effects and relative impacts differ between the two channel proteins.

Materials and Methods

Molecular genetics and expression

SKOR and KAT1 mutation, expression and analysis used standard molecular genetic methods. Site mutations and chimera constructs were generated as described previously (Poree *et al.*, 2005; Johansson *et al.*, 2006). All mutants were verified by sequencing. For expression, the coding regions of wild-type and mutant channels were cloned into the vector pGEMHE, and cRNA was synthesized using T7 polymerase (mMessage mMachine, Ambion Europe Ltd, Huntingdon, UK). For expression in oocytes, stage V and VI oocytes were taken from *Xenopus laevis* and maintained at 18°C in a modified Barth's medium containing (in mM) 96 NaCl, 2 KCl, 1 $CaCl_2$, 1 $MgCl_2$ and 10 HEPES/NaOH (pH 7.4). Oocytes were defolliculated by collagenase treatment (2 mg ml^{-1}, type IA, No. C9891, Sigma, Taufkirchen, Germany). Defolliculated oocytes were injected with 40 ng (1 μg μl^{-1}) cRNA using a solid displacement injector (Picospritzer III, Parker Instrumentation, Fairfield, NJ, USA) and kept at 18–20°C. Control oocytes were injected with 40 nl of deionized water.

Electrophysiology

Whole-cell currents were measured under voltage clamp (Turbo TEC-10CX; NPI Electronic, Tamm, Germany) with a two-electrode clamp circuit and virtual ground. Voltage control, data acquisition, and data analyses were carried out using the Pulse/PulseFit software (HEKA, Lambrecht/Pfalz, Germany). Measurements were performed in bath solutions containing (in mM) 1 $CaCl_2$ and 2 $MgCl_2$, buffered with 10 Tris/MES, pH 7.4, with the addition of (in mM): K3, 3 KCl and 97 NaCl; K10, 10 KCl and 90 NaCl; K30, 30 KCl and 70 NaCl; and K100, 100 KCl. Measurements were repeated routinely at the end of each treatment with the addition of 10 mM CsCl to distinguish K^+ currents and any background, nonselective leak. In experiments testing very negative voltages (< −170 mV) 1 mM $LaCl_3$ was added to the bath solution to efficiently suppress possible endogenous currents at these voltages (Naso *et al.*, 2006). The presence of La^{3+} had no detectable adverse effect on the investigated K^+ channels.

Data analysis

To standardize comparisons of wild-type with mutant channel currents, relative conductances were obtained in two-step pulse experiments. In a first pulse (variable voltage V), channels were activated followed by a tail-pulse (nonvariable voltage V_T). The current measured at the end of the first pulse is the steady-state current I_{SS}. The current measured at the onset of the tail-pulse, tail current I_T, can be expressed as $I_T(V) = N \times i(V_T) \times P_{open}(V)$, where $P_{open}(V)$ is the open probability of the channel at the end of the first pulse. Thus, the tail current is proportional to the open probability $P_{open}(V)$. The resulting curves were fitted such that:

$$I_T(V) = I_{max}/[1 + \exp(-(V - V_{1/2})/V_S)] + \text{offset} \qquad \text{Eqn 1}$$

where I_{max} is the maximum current, V is the voltage of the activation pulse, $V_{1/2}$ is the voltage giving half-maximal conductance, V_S is the voltage sensitivity coefficient, the parameter offset is a constant. Fittings were carried out using a Marquardt–Levenberg algorithm (Marquardt, 1963) and the resulting values for I_{max} and offset used to calculate relative conductances $\text{rel.}G = [I_T(V) - \text{offset}]/I_{max}$. Current records were corrected for background current, estimated as a linear leak component from measurements between −130 and −160 mV after substituting Cs^+ for K^+ to block the K^+ channels. Measurements were discarded when the maximum leak current exceeded 5% of the maximum current in the steady state. To describe gating with a two-state model and to quantify the energy difference between open and closed states, ΔG_{OC}, a Boltzmann function was fitted to the $\text{rel.}G(V)$ values:

$$\text{rel.}G(V) = \frac{1}{1 + e^{-\left(\frac{\Delta G_{OC}}{kT}\right)}} = \frac{1}{1 + e^{-z\frac{e_0}{kT}(V - V_{1/2})}} \qquad \text{Eqn 2}$$

resulting in $\Delta G_{OC} = z \times e_0 \times (V - V_{1/2})$ values which could be compared as $\Delta(\Delta G) = \Delta G_{OC}{}^{\text{mutant}} - \Delta G_{OC}{}^{\text{wild-type}}$. z is the apparent gating charge and e_0 is the elementary charge, and k and T have their usual meanings. To reduce the number of free parameters, fits were constrained by the adjustment of a common value z for all KAT1- and SKOR-based datasets, respectively. Results are reported as means ± standard deviation where appropriate.

Molecular models for KAT1 and SKOR channels

KAT1 and SKOR homology models (in open and closed state) were built using ICM software (Abagyan *et al.*, 1994). The template to build the homology models was the α-subunit of the Kv1.2 model obtained by the Rosseta method (Yarov-Yarovoy *et al.*, 2006a,b). The multiple alignment used to build KAT1 and SKOR models is based on two alignments previously published by Pathak *et al.* (2007) and Poree *et al.* (2005). Homology models of KAT1 and SKOR were validated using PROCHECK (Laskowski *et al.*, 1993). The structural models of KAT1 (open and closed states) contain 220 amino acids, while those of SKOR comprise 216 amino acids. KAT1 and SKOR homology models contain the S1–S6 transmembrane segments; the S2–S3 and S5–S6 loops were not included in the models. For each model the tautomeric states of histidine residues were assigned according to the local environment using the VMD plugin 'check side chains' (http://imr.cnrs-mrs.fr/IMR/our_softs.htm).

KAT1 and SKOR homology models were embedded into a pre-equilibrated phosphatidyl oleoyl phosphatidylcholine (POPC) bilayer in a periodic boundary condition box ($13.3 \times 13.23 \times 9.03$ nm) with pre-equilibrated TIP3P water molecules (Jorgensen *et al.*, 1983). Three K^+ ions were associated to the models in positions S0, S2 and S4 of the selectivity filter (Aqvist & Luzhkov, 2000). Other K^+ ions were placed in the intracellular vestibule according to experimentally determined sites for K^+ ions obtained in the crystallographic structure of the KcsA channel (PDB: 1K4C; Zhou *et al.*, 2001). An average of 13 potassium ions was added to the aqueous phase to simulate a concentration of 50 mM K^+. An average of 37 chloride ions was added for electroneutrality. The initial configurations of the systems were first optimized using energy minimization with a progressive decrease of harmonic restraints applied to the backbone atoms. Minimization was followed by an equilibration step using a molecular dynamics (MD) simulation at 298 K for 1 ns. All molecular dynamic simulations were performed using the NAMD program (Phillips *et al.*, 2005). The electrostatic interactions were computed with no truncations using the particle mesh Ewald algorithm (Essmann *et al.*, 1995) under periodic boundary conditions. Pore cavity diameters in SKOR and KAT1 were analyzed in open and closed states by using the method HOLE (Smart *et al.*, 1996).

Results

A sequence alignment of the S6 α-helices of the inward- (K_{in}) and outward-rectifying (K_{out}) K^+ channel subfamilies of *Arabidopsis* and homologs from *Populus*, maize and grape highlights their close similarities, notably within the central and C-terminal regions of the helix (Fig. 1). Over this stretch of 18 amino acid residues, KAT1 and SKOR share 66% identity and retain virtually complete identity with other members of their respective subfamilies. Of the residue differences, six positions (Fig. 1, positions numbered 1–6) clearly distinguish the two Kv channel subfamilies. Several of these residues were previously identified to affect the rectification (Poree *et al.*, 2005) and K^+ sensitivity (Johansson *et al.*, 2006) of SKOR, implicating their significance for the differences in the gating characteristics of these two channel subfamilies, but less information was available for KAT1. We therefore undertook a systematic analysis of this portion of the S6 helices of KAT1 and SKOR, through symmetric domain

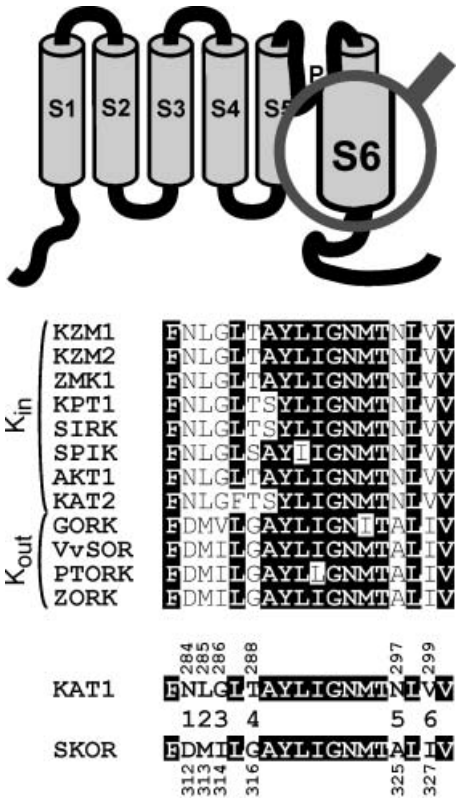

Fig. 1 Sequence comparison of the C-terminal halves of the S6 helices of plant inward-rectifying (K_{in}) and outward-rectifying (K_{out}) channels. Inward-rectifying K^+ channels KZM1, KZM2, ZMK1 from *Zea mays*, KPT1 from *Populus tremula* × *Populus tremuloides*, SIRK from *Vitis vinifera*, SPIK, AKT1, KAT2, and KAT1 from *Arabidopsis thaliana*, and outward-rectifying K^+ channels SKOR, GORK from *Arabidopsis thaliana*, VvSOR from *Vitis vinifera*, PTORK from *Populus tremula* × *Populus tremuloides*, and ZORK from *Zea mays*. Residues differing between KAT1 (inward-rectifier, K_{in} channel) and SKOR (outward-rectifier, K_{out} channel) are highlighted (positions 1, 2, 3, 4, 5, and 6) and were targeted in site-directed mutagenesis experiments.

swapping and single residue exchanges between the two K^+ channels and analysis of the resultant chimeras and mutants after heterologous expression in *Xenopus* oocytes.

S6 exchange uncovers functional asymmetries between KAT1 and SKOR

Swapping the entire central and C-terminal domains of the S6 helices between KAT1 and SKOR had very different and nonsymmetric effects on the gating of the two K^+ channels. The SKOR K^+ channel normally rectifies strongly outward, activating on membrane depolarization and in a time- and K^+-dependent manner (Fig. 2a–c). By contrast, the mutant SKOR-$S6_{KAT1(1–6)}$ (=SKOR-D312N-M313L-I314G-G316T-A325N-I327V) appeared to be a K^+-selective leak without evidence of the relatively fast kinetic relaxations normally associated with channel (de-)activation (Fig. 2d,e). These observations indicated that the substitutions greatly reduced the activation energy needed to open the SKOR K^+ channel. The substitution strongly modified the voltage dependence and inverted the K^+ dependence of gating. Whereas a high concentration of external K^+ suppressed the currents in the wild-type by shifting the activation threshold of the channel to a more positive voltage (Johansson *et al.*, 2006), in the chimera it promoted channel activation (Fig. 2f). At membrane voltages less than –200 mV we observed very slow current deactivations in 10 mM K^+, which were not observed in 30 mM K^+, indicating channel deactivation (or inactivation) in the presence of 10 mM but not 30 mM K^+. For these experiments, we added 1 mM $LaCl_3$ to the bath solution to suppress endogenous currents (Naso *et al.*, 2006).

The KAT1 K^+ channel normally rectifies strongly inward, activating on membrane hyperpolarization, but with a voltage-dependence of gating that is independent of $[K^+]_o$ (Fig. 2g–j). Replacing the central and C-terminal domains of the S6 α-helix of KAT1 with that of SKOR, KAT1-$S6_{SKOR(1–6)}$ (=KAT1-N284D-L285M-G286I-T288G-N297A-V299I) yielded KAT1 channel current, but at voltages displaced approx. –110 mV relative to the wild-type KAT1 (Fig. 2k–m). Over the voltage range from +20 mV to –160 mV the KAT1-$S6_{SKOR(1–6)}$ mutant remained silent; the current was demonstrable only at voltages approaching –200 mV and was verified by its sensitivity to block by extracellular Cs^+ (not shown). Otherwise, the KAT1-$S6_{SKOR(1–6)}$ current, like that of KAT1, increased with $[K^+]_o$ (Fig. 2l), while the relative conductance (gating) of the channels showed no sensitivity to external K^+ concentration (Fig. 2m). Only the static voltage displacement – and, hence, the energy required to activate the KAT1-$S6_{SKOR(1–6)}$ mutant – was increased relative to the wild-type KAT1 K^+ channel. We quantified the gating of KAT1 and its mutant using a simple two-state model (Michard *et al.*, 2005b). The analysis showed an energy increase of $\Delta(\Delta G) = 5.8 \pm 0.6\ kT$ for KAT1-$S6_{SKOR(1–6)}$ (Table 1). Thus, exchanging the corresponding S6 domains of KAT1 and of SKOR had markedly different effects on gating of the two K^+ channels: whereas the SKOR-$S6_{KAT1(1–6)}$ mutant showed profound and qualitative alterations of the voltage and K^+ dependencies to its gating, the KAT1-$S6_{SKOR(1–6)}$ mutant was affected quantitatively in its gating energy barrier but qualitatively showed all of the gating characteristics of the wild-type channel in relation to extracellular K^+.

Mutations in the centre of S6 primarily affect the gating of SKOR

The S6 regions of KAT1 and SKOR share a large sequence in common and differ primarily at the limits of this stretch of residues, thereby allowing subdivision of the S6 helix into two parts. The first part (Fig. 1, positions 1–4) is localized in the centre of the S6 helix and has been identified in SKOR as a so-called S6 gating domain (Johansson *et al.*, 2006). The

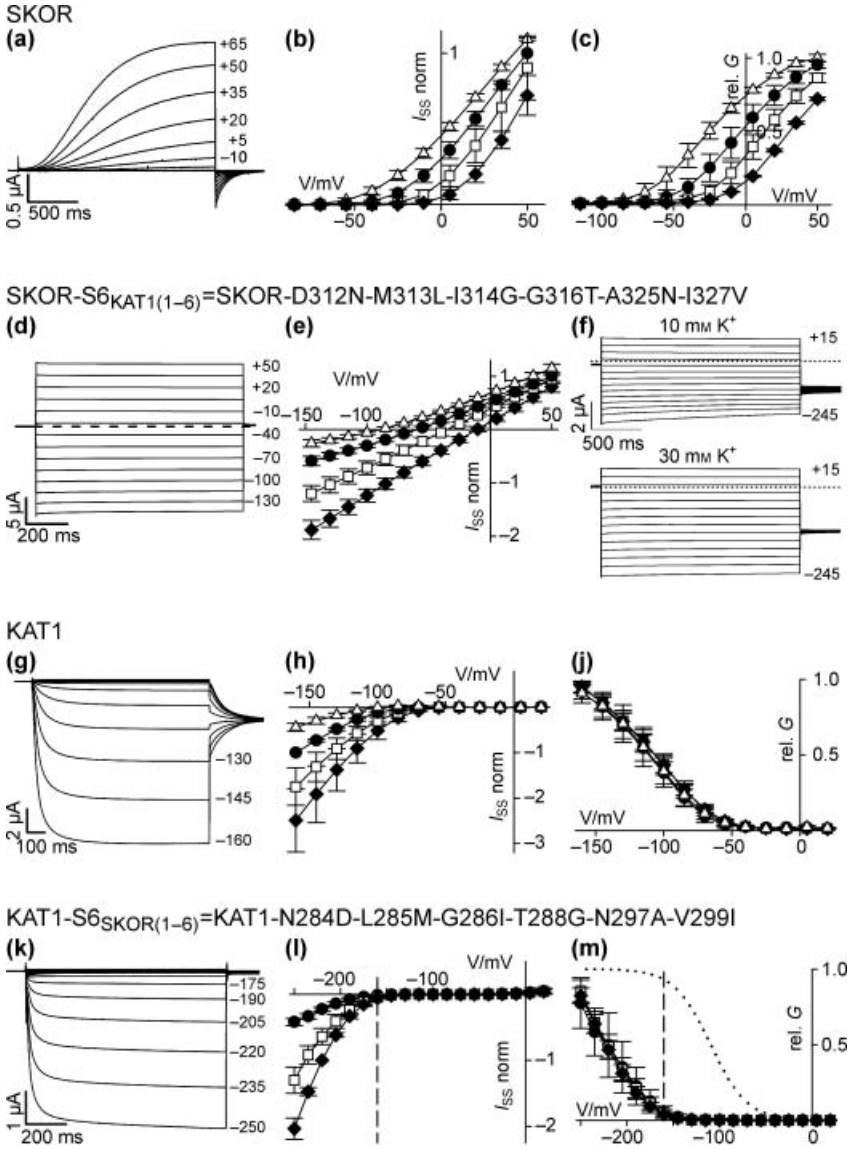

Fig. 2 Swapping of the C-terminal halves of the S6 segments (positions 1, 2, 3, 4, 5, 6) affects SKOR and KAT1 differently. (a–c) Characteristics of the SKOR wild-type. (a) Representative K^+ currents recorded in 10 mM K^+ during 2 s voltage steps from –100 mV to voltages between –85 mV and +65 mV (15 mV increments) followed by a final step to –100 mV. (b) Steady-state current-voltage curves; and (c) relative conductance for wild-type SKOR ($n = 5$). (d–f) Swapping of the C-terminal half of the S6 segment from KAT1 to SKOR eliminates outward rectification. Characteristics of the mutant SKOR-D312N-M313L-I314G-G316T-A325N-I327V (=SKOR with the C-terminal half of the KAT1-S6 segment). (d) Representative K^+ currents recorded in 10 mM K^+ during 1 s voltage steps from –30 mV to voltages between –145 mV and +50 mV (15 mV increments) followed by a final step to –30 mV (zero current, dashed line). (e) Steady-state current–voltage curves ($n = 4$). (f) Representative K^+ currents recorded in 10 mM K^+ (upper traces) and 30 mM K^+ (lower traces) during 2 s voltage steps from –62 mV (10 mM K^+) and –27 mV (30 mM K^+), respectively, to voltages between –245 mV and +15 mV (15 mV increments) followed by a final step to –140 mV (zero current, dotted lines). Scale bars refer to both. Data are representative for at least three independent experiments. (g–j) Characteristics of the KAT1 wild-type. (g) Representative K^+ currents recorded in 10 mM K^+ during 1 s voltage steps from –40 mV to voltages between –160 mV and +20 mV (15 mV increments) followed by a final step to –110 mV. (h) Steady-state current-voltage curves; and (j) relative conductance for wild-type KAT1 ($n = 4$). (k–m) Swapping of the C-terminal half of the S6 segment from SKOR to KAT1 shifts the activation threshold to more negative voltages. Characteristics of the mutant KAT1-N284D-L285M-G286I-T288G-N297A-V299I (=KAT1 with the C-terminal half of the SKOR-S6 segment). (k) Representative K^+ currents recorded in 100 mM K^+ during 2 s voltage steps from –20 mV to voltages between –250 mV and +20 mV (15 mV increments) followed by a final step to –60 mV. (l) Steady-state current–voltage curves; and (m) relative conductance ($n = 5$). Data were recorded in 3 (triangles), 10 (circles), 30 (squares), and 100 mM K^+ (diamonds). Data in (b) and (e) were normalized between experiments to values measured in 10 mM K^+ at +50 mV; data in (h) to values measured in 10 mM K^+ at –160 mV and data in (l) to values measured in 100 mM K^+ at –220 mV. The dotted line in (m) indicates the relative conductance of wild-type KAT1. The dashed lines in (l) and (m) indicate –160 mV, the most negative voltage usually tested for the KAT1 wild-type. In (a), (d), (f), (g) and (k) the step-voltage is indicated in mV for selected traces.

Table 1 Summary of mutants in the S6 region analyzed in this study

Position[a]	Channel	Chimera/mutation	Effect
1, 2, 3, 4, 5, 6	SKOR	D312N-M313L-I314G-G316T-A325N-I327V	Inverted K^+-sensitivity, →(–)
	KAT1	N284D-L285M-G286I-T288G-N297A-V299I	→(–), $\Delta(\Delta G) = 5.8 \pm 0.6\ kT$
1, 2, 3, 4	SKOR	D312N-M313L-I314G-G316T	No rectification[b]
	KAT1	N284D-L285M-G286I-T288G	→(–), $\Delta(\Delta G) = 1.9 \pm 0.5\ kT$
5, 6	SKOR	A325N-I327V	No current[b]
	KAT1	N297A-V299I	→(–), $\Delta(\Delta G) = 6.4 \pm 0.6\ kT$
2, 5, 6	KAT1	L285M-N297A-V299I	→(–), $\Delta(\Delta G) = 3.5 \pm 0.5\ kT$
1	SKOR	D312N	Inverted K^+-sensitivity[c]
	KAT1	N284D	Similar to WT, $\Delta(\Delta G) = 0.4 \pm 0.4\ kT$
2	SKOR	M313L	No K^+ sensitivity;
			→(–), $\Delta(\Delta G) = -3.8 \pm 0.5\ kT$[cd]
	KAT1	L285M	→(+), $\Delta(\Delta G) = -4.2 \pm 0.3\ kT$
3	SKOR	I314G	→(–), $\Delta(\Delta G) = -6.6 \pm 0.7\ kT$[c]
	KAT1	G286I	→(–), $\Delta(\Delta G) = 2.0 \pm 0.5\ kT$
4	SKOR	G316T	→(+), $\Delta(\Delta G) = 2.0 \pm 0.6\ kT$[c]
	KAT1	T288G	→(–), $\Delta(\Delta G) = 2.1 \pm 0.5\ kT$
5	KAT1	N297A	→(–), $\Delta(\Delta G) = 5.7 \pm 0.6\ kT$
6	SKOR	A325S-I327V	Similar to WT, $\Delta(\Delta G) = 0.5 \pm 0.6\ kT$
	KAT1	V299I	→(–), $\Delta(\Delta G) = 2.1 \pm 0.7\ kT$

The label '→(–)' indicates a shift of the activation threshold to more negative voltages when compared with the wild-type. This is equivalent to an increase of the activation energy in KAT1 mutants and a decrease of the activation energy in SKOR mutants. The label '→(+)' indicates a shift of the activation threshold to more positive voltages when compared with the wild-type. This is equivalent to a decrease of the activation energy in KAT1 mutants and an increase of the activation energy in SKOR mutants.
[a]See Fig. 1.
[b]Tested voltage range –150 to +80 mV.
[c]Data published earlier (Johansson *et al*., 2006).
[d]Determined in 10 mM K^+.

second part (Fig. 1, positions 5–6) is located at the cytosolic end of the S6 helix. To elucidate further the roles of the different parts of S6, we swapped these smaller regions. Substitution of the entire central segment of SKOR by that of KAT1 eliminated the rectification of the channel in the investigated voltage interval. The mutant SKOR-$S6_{KAT1(1–4)}$ (=SKOR-D312N-M313L-I314G-G316T), like SKOR-$S6_{KAT1(1–6)}$, was characterized by instantaneous currents (Fig. 3a) and linear current-voltage curves (Fig. 3b) consistent with a K^+-selective, open channel. SKOR-$S6_{KAT1(1–4)}$ and SKOR-$S6_{KAT1(1–6)}$ showed the same characteristics as the triple mutant SKOR-$S6_{KAT1(1–3)}$ (=SKOR-D312N-M313L-I314G) (Poree *et al*., 2005; Johansson *et al*., 2006), indicating that the properties of chimeric substitutions with the KAT1 S6 sequence are dominated by the effects of substitutions at residue positions 1, 2 and 3. Analysis of the chimeric KAT1 mutant incorporating the central S6 region from the SKOR sequence showed no qualitative effect on KAT1 gating. Current characteristics of the KAT1-$S6_{SKOR(1–4)}$ (=KAT1-N284D-L285M-G286I-T288G) mutant were very similar to KAT1, albeit with a moderate negative shift of approx. –35 mV in $V_{1/2}$, the characteristic voltage yielding half-maximal activation (Fig. 3c–e). Thus, by contrast with SKOR, the effects of substitutions within KAT1 appeared not to be dominated by a central S6 gating domain. Instead, KAT1 gating was dominated by mutations at the end of the S6 helix.

Mutation at the S6 C-terminus dominate KAT1 gating

Our previous study of the SKOR S6 gating domain showed that the gating properties of multiple residue substitutions were not always easily reconciled with the characteristics of single mutations at the individual residues, that is, SKOR-$S6_{KAT1(1)}$ (=SKOR-D312N), SKOR-$S6_{KAT1(2)}$ (=SKOR-M313L), SKOR-$S6_{KAT1(3)}$ (=SKOR-I314G), and SKOR-$S6_{KAT1(4)}$ (=SKOR-G316T), or with a summation of their properties (Johansson *et al*., 2006). We were interested, therefore, to determine whether the same was true for corresponding substitutions in KAT1 or whether the effects of the KAT1-$S6_{SKOR(1–6)}$ chimera could be associated primarily with mutation of a single residue. Table 1 and Supporting Information Fig. S1 summarize measurements from oocytes expressing KAT1 mutants with single substitutions at each of the first four sites (see Fig. 1) in the centre of the S6 helix. For three of the four mutants – KAT1-$S6_{SKOR(1)}$ (=KAT1-N284D) (Fig. S1a–c), KAT1-$S6_{SKOR(3)}$ (=KAT1-G286I) (Fig. S1g–j) and KAT1-$S6_{SKOR(4)}$ (=KAT1-T288G) (Fig. S1k–m) – substitutions with the corresponding residues from SKOR yielded ensemble currents and conductance characteristics that differed little from the wild-type KAT1 K^+ channel. In each case, currents were observed to activate over periods of *c*. 200 ms with steps from a holding voltage of –20 mV to voltages near and negative of –100 mV, and steady-state

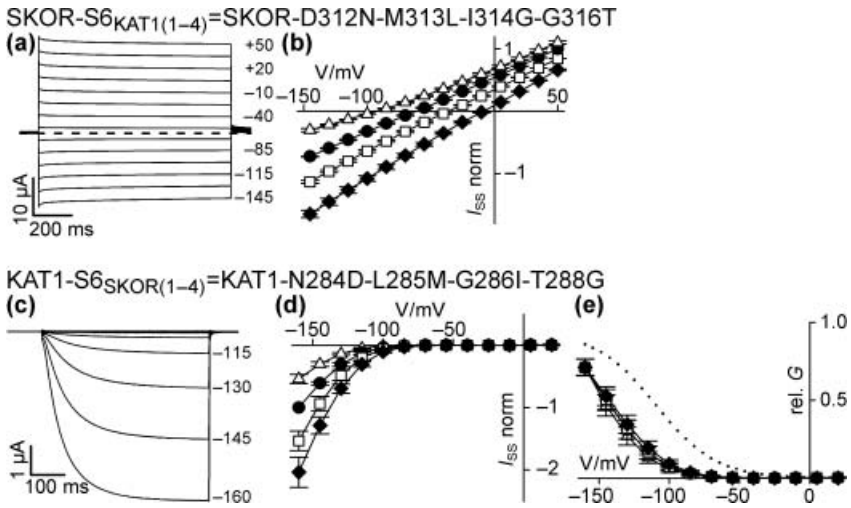

Fig. 3 Swapping of the central part of the S6 helix (positions 1, 2, 3, 4) strongly affects SKOR but barely affects KAT1. (a, b) Swapping of the central part of the S6 segment from KAT1 to SKOR eliminates outward rectification. Characteristics of the mutant SKOR-$S6_{KAT1(1–4)}$ (=SKOR-D312N-M313L-I314G-G316T). (a) Representative K^+ currents recorded in 10 mM K^+ during 1 s voltage steps from –60 mV to voltages between –145 mV and +50 mV (15 mV increments) followed by a final step to –60 mV (zero current, dashed line). (b) Steady-state current-voltage curves ($n = 3$). (c–e) Swapping of the central part of the S6-segment from SKOR to KAT1 slightly shifted the activation threshold. Characteristics of the mutant KAT1-$S6_{SKOR(1–4)}$ (=KAT1-N284D-L285M-G286I-T288G). (c) Representative K^+ currents recorded in 10 mM K^+ during 1 s voltage steps from –20 mV to voltages between –160 mV and +20 mV (15 mV increments) followed by a final step to –60 mV. (d) Steady-state current–voltage curves; and (e) relative conductance ($n = 11$). Data were recorded in 3 (triangles), 10 (circles), 30 (squares), and 100 mM K^+ (diamonds). Data in (b) were normalized between experiments to values measured in 10 mM K^+ at +50 mV and in (d) to values measured in 10 mM K^+ at –160 mV. The dotted line in (e) indicates the relative conductance of wild-type KAT1. In (a) and (c) the step-voltage is indicated in mV for selected traces.

current-voltage curves showed a pronounced inward rectification and scalar increase in current with $[K^+]_o$. Like the wild-type current, relative conductances showed no evidence of a K^+ sensitivity of the voltage-dependence of gating. Only for the KAT1-$S6_{SKOR(2)}$ (=KAT1-L285M) mutant (Table 1, Fig. S1d–f) was the residue substitution found to alter gating appreciably. However, the effect was to displace its voltage dependence *c.* +100 mV relative to wild-type KAT1. In other words, neither individual site substitutions within the first four sites (Fig. 1) nor the quadruple mutant KAT1-$S6_{SKOR(1–4)}$ showed any evidence of the pronounced negative voltage shift in gating observed with the KAT1-$S6_{SKOR(1–6)}$ chimera (see earlier).

To analyze the effects of residue substitutions at the C-terminal end of the KAT1 S6 helix, sites 5 and 6 (Fig. 1), we followed a similar approach as for the central S6 region. Expressing the double mutant KAT1-$S6_{SKOR(5–6)}$ (=KAT1-N297A-V299I) in oocytes reproduced essentially all of KAT1-$S6_{SKOR(1–6)}$ behavior (Fig. 4a–c), notably the pronounced negative shift of the relative conductance characteristics. We also expressed the individual site substitutions in separate experiments. For the KAT1-$S6_{SKOR(5)}$ (=KAT1-N297A) mutant, current records yielded quantitatively similar results, with the ensemble current activating noticeably only at voltages negative from −160 mV, irrespective of the prevailing $[K^+]_o$, and best fittings giving an apparent $V_{1/2}$ for the current near −220 mV (Fig. 4d–f). For the KAT1-$S6_{SKOR(6)}$ (=KAT1-V299I) mutant, recordings uncovered a current similar to that of the wild-type KAT1, albeit with the relative conductance characteristic shifted marginally to more negative voltages (Fig. 4g–j). Complementary substitutions in the SKOR S6 helix failed to yield any measurable current in the SKOR-$S6_{KAT1(5–6)}$ (=SKOR-A325N-I327V) double mutant (Fig. 5a). However, this apparently lethal defect was not observed with a more conservative substitution at position 5. The mutant SKOR-$S6_{KAT1(*6)}$ (=SKOR-A325S-I327V) showed characteristics similar to the wild-type (Fig. 5b–d), indicating a dominant role of the substitution A325N and a minor role of I327V in determining the features of the SKOR-$S6_{KAT1(5–6)}$ double mutant. *In toto*, these studies demonstrate a special role of the position 5 (Fig. 1) in the gating of KAT1 and SKOR. In KAT1, this role was especially pronounced because the KAT1-$S6_{SKOR(1–6)}$ characteristics were dominated by mutation of the single KAT1 residue N297. Substitution at this position also masked, in part, the effects of the KAT1-$S6_{SKOR(2)}$ mutation (Fig. 4k–m). Whereas in the wild-type background the mutation at position 2 reduced the activation energy of the channel by 4.2 *kT*, the same substitution did only by *c.* 2.9 *kT* in the mutant KAT1-$S6_{SKOR(5–6)}$ background. Fig. 6 and Table 1 summarize these and related observations from complementary S6-helix residue exchanges between KAT1 and SKOR.

Structural models for SKOR and KAT1

To gain further insights into the gating of KAT1 and SKOR, we were interested to compare the differences in structural arrangements between the open and the closed states in both

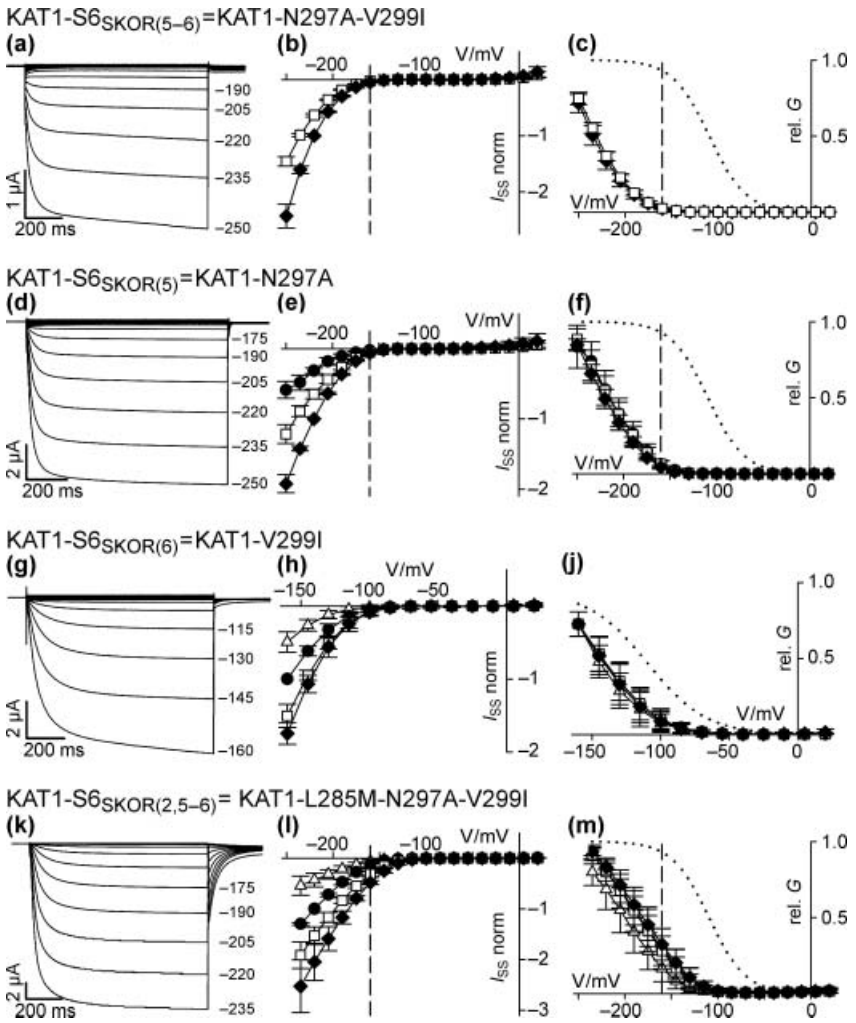

Fig. 4 Swapping of the final part of the S6 helix (positions 5, 6) from SKOR to KAT1. (a–c) Swapping at positions 5 and 6 from SKOR to KAT1 shifts the activation threshold of KAT1 to more negative voltages. Characteristics of the mutant KAT1-$S6_{SKOR(5–6)}$ (=KAT1-N297A-V299I). (a) Representative K^+ currents recorded in 100 mM K^+ during 1 s voltage steps from –20 mV to voltages between –250 mV and +20 mV (15 mV increments) followed by a final step to –60 mV. (b) Steady-state current–voltage curves; and (c) relative conductance (n = 3). (d–f) Swapping at position 5 shifts the activation threshold of KAT1 to more negative voltages. Characteristics of the mutant KAT1-$S6_{SKOR(5)}$ (=KAT1-N297A). (d) Representative K^+ currents recorded in 100 mM K^+ during 1 s voltage steps from –20 mV to voltages between –250 mV and +20 mV (15 mV increments) followed by a final step to –60 mV. (e) Steady-state current–voltage curves; and (f) relative conductance (n = 5). (g–j) Swapping at position 6 did not strongly affect the gating of KAT1. Characteristics of the mutant KAT1-$S6_{SKOR(6)}$ (=KAT1-V299I). (g) Representative K^+ currents recorded in 10 mM K^+ during 1 s voltage steps from –20 mV to voltages between –160 mV and +20 mV (15 mV increments) followed by a final step to –60 mV. (h) Steady-state current–voltage curves; and (j) relative conductance (n = 4). (k–m) The additional exchange L285M poorly rescues the negative shift of the activation threshold induced by the N297A-V299I exchanges. Characteristics of the mutant KAT1-$S6_{SKOR(2,5–6)}$ (=KAT1-L285M-N297A-V299I). (k) Representative K^+ currents recorded in 100 mM K^+ during 1 s voltage steps from –20 mV to voltages between –235 mV and +20 mV (15 mV increments) followed by a final step to –130 mV. (l) Steady-state current-voltage curves; and (m) relative conductance (n = 4). Data were recorded in 3 (triangles), 10 (circles), 30 (squares), and 100 mM K^+ (diamonds). Values in (b) and (e) were normalized between experiments to values measured in 100 mM K^+ at –220 mV, in (h) to values measured in 10 mM K^+ at –160 mV, and in (l) to values measured in 10 mM K^+ at –220 mV. In (a), (d), (g), and (k), the step-voltage is indicated in mV for selected traces. The dashed lines in (b), (c), (e), (f), (l), and (m) indicate –160 mV, the most negative voltage usually tested for the KAT1 wild-type. The dotted lines in (c), (f), (j), and (m) indicate the relative conductance of wild-type KAT1.

channels. In the absence of crystal structure data we were obliged to approximate the channel structures by homology modeling. As a template we used the models of the Kv1.2 channel that were built with the Rosetta method for membrane proteins (Yarov-Yarovoy *et al.*, 2006b). The models of the Kv1.2 channel are currently the only structures of a potassium channel in the open and in the closed state (Yarov-Yarovoy *et al.*, 2006a). Comparison of the model of Kv1.2 in the open state obtained by Rosetta with the native crystallographic structure of Kv1.2 (Long *et al.*, 2005) revealed a mean square

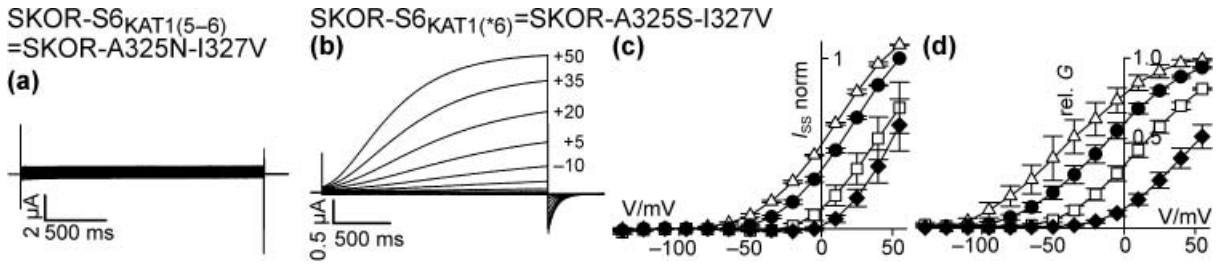

Fig. 5 Swapping of the final part of the S6 helix (positions 5, 6) eliminates SKOR currents. (a) The mutant SKOR-$S6_{KAT1(5-6)}$ (=SKOR-A325N-I327V) does not open in the tested voltage interval. Representative K^+ currents recorded in 10 mM K^+ during 2 s voltage steps from –70 mV to voltages between –145 mV and +50 mV (15 mV increments) followed by a final step to –70 mV. (b–d) The mutant SKOR-$S6_{KAT1(*6)}$ (=SKOR-A325S-I327V) is similar to the SKOR wild-type. (b) Representative K^+ currents recorded in 10 mM K^+ during 2 s voltage steps from –75 mV to voltages between –145 mV and +50 mV (15 mV increments) followed by a final step to –140 mV. For selected traces, the step-voltage is indicated in mV. (c) Steady-state current-voltage curves recorded in 3 (triangles), 10 (circles), 30 (squares), and 100 mM K^+ (diamonds). Data of three cells normalized between experiments to values measured in 10 mM K^+ at +55 mV. (d) Relative conductance determined as described in the Materials and Methods section on 'Data analysis'. Symbols as in (c).

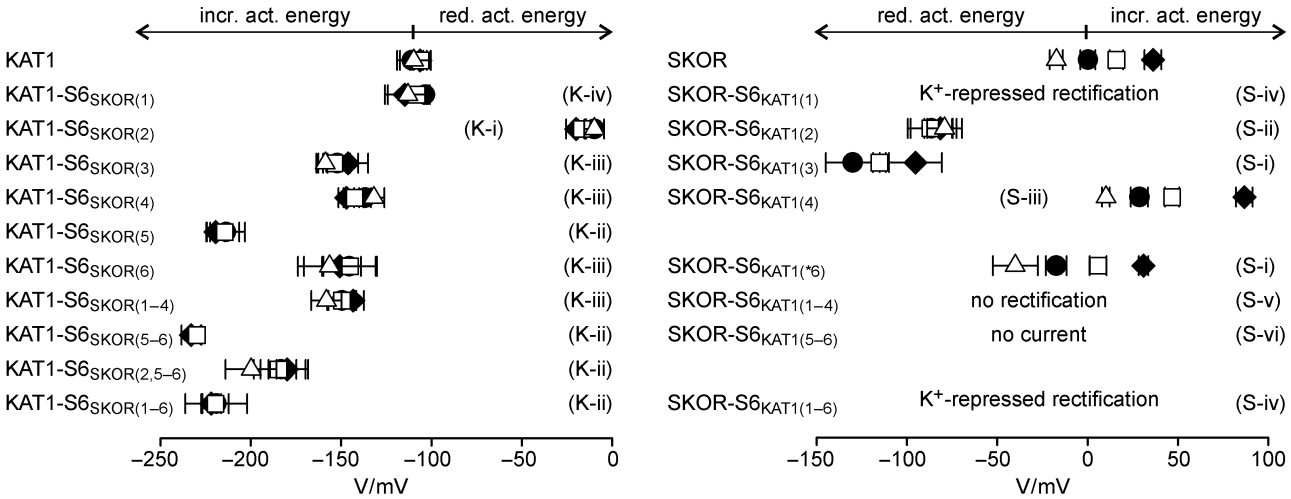

Fig. 6 Mutations in S6 affect the gating of KAT1 and SKOR. Half-maximal activation voltages ($V_{1/2}$) of the mutants tested in this study. The $V_{1/2}$ values were separately determined for 3 mM K^+ (triangles), 10 mM K^+ (circles), 30 mM K^+ (squares), and 100 mM K^+ (diamonds). n = 3–11. Mutations in the C-terminal half of the S6 segment of KAT1 had four different effects: (K-i) they strongly reduced the energy needed to activate the channel ('red. act. energy') – this is equivalent to a pronounced positive shift of $V_{1/2}$ along the voltage-axis (KAT1-$S6_{SKOR(2)}$); (K-ii) they strongly increased the energy needed to activate the channel ('incr. act. energy') – this is equivalent to a pronounced negative shift of $V_{1/2}$ along the voltage-axis (KAT1-$S6_{SKOR(5)}$, KAT1-$S6_{SKOR(5–6)}$, KAT1-$S6_{SKOR(2,5–6)}$, KAT1-$S6_{SKOR(1–6)}$); (K-iii) they slightly increased the energy needed to activate the channel ('incr. act. energy'; moderate negative shift of $V_{1/2}$ along the voltage axis (KAT1-$S6_{SKOR(3)}$, KAT1-$S6_{SKOR(4)}$, KAT1-$S6_{SKOR(6)}$, KAT1-$S6_{SKOR(1-4)}$); or (K-iv) they left the gating properties largely unaffected (KAT1-$S6_{SKOR(1)}$). Mutations in the C-terminal half of the S6 segment of SKOR had six different effects: (S-i) they reduced the energy needed to activate the channel ('red. act. energy'; negative shift of $V_{1/2}$ along the voltage-axis) and left the K^+ dependence of the gating unaffected (SKOR-$S6_{KAT1(3)}$, SKOR-$S6_{KAT1(*6)}$); (S-ii) they reduced the energy needed to activate the channel ('red. act. energy'; negative shift of $V_{1/2}$ along the voltage axis) and almost eliminated the K^+ dependence of the gating (SKOR-$S6_{KAT1(2)}$); (S-iii) they increased the energy needed to activate the channel ('incr. act. energy'; positive shift of $V_{1/2}$ along the voltage-axis) and left the K^+ dependence of the gating unaffected (SKOR-$S6_{KAT1(4)}$); (S-iv) they inverted the K^+ sensitivity of the gating (SKOR-$S6_{KAT1(1)}$, SKOR-$S6_{KAT1(1–6)}$); (S-v) they locked the channels open, probably by reducing greatly the energy needed to activate the channel, and probably inverted the K^+ sensitivity (SKOR-$S6_{KAT1(1–4)}$); (S-vi) they locked the channels closed, probably by greatly increasing the energy needed to activate the channel (SKOR-$S6_{KAT1(5–6)}$).

deviation (RMSD) of only 2.0 Å (Yarov-Yarovoy *et al.*, 2006a). Therefore, the model of the closed Kv1.2 channel obtained by Rosetta is nowadays also widely accepted (Mashl & Jakobsson, 2008), although the crystallographic structure of the closed Kv1.2 has not yet been obtained.

Modeling of KAT1 and SKOR suggested that structural rearrangements during gating are different in both channels. We analyzed the pore dimensions of KAT1 and SKOR in the open and closed states after equilibration in the membrane using the method HOLE (Smart *et al.*, 1996) (Fig. 7). This algorithm employs a Monte Carlo simulated annealing procedure to find the best route for a sphere with variable radius to squeeze through the channel. The analyses revealed that during the closing process the permeation pathway of

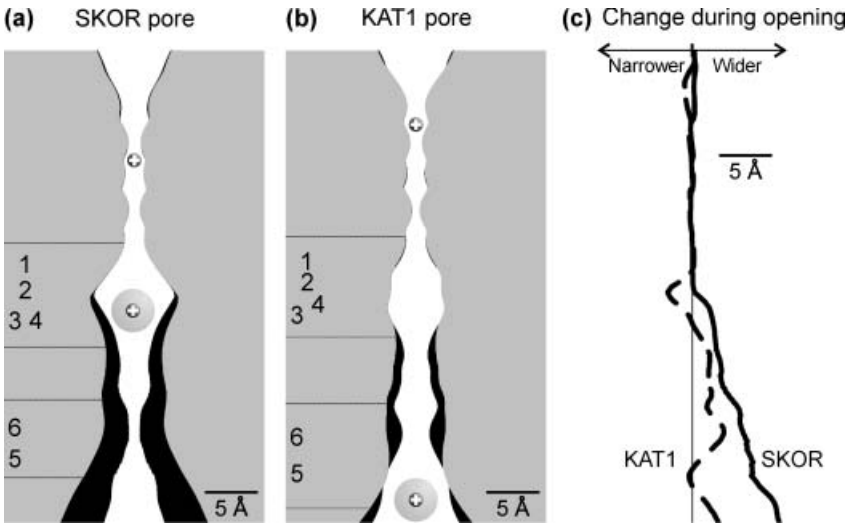

Fig. 7 Structural computational simulation of the permeation pathway. (a, b) Cross-section of the SKOR channel (a) and the KAT1 channel (b) in the closed state (black) and in the open state (gray) in a side view. Potassium ions (+) are dehydrated in the selectivity filter and surrounded by a hydration shell (gray sphere) in the pore cavity and in the vestibules. Numbers indicate the locations of positions 1–6, while dotted lines indicate the dimensions of the proximal (positions 1–4) and distal regions (positions 5–6) in S6. (c) Change of the width of the permeation pathway during opening in SKOR (solid line) and KAT1 (dashed line). The vertical line indicates 0 Å, that is, no change of the pore diameter. Scale bars refer to all dimensions, *x*/*y* and *z*.

SKOR narrows down at the cytosolic end of the channel, whereas the rest of the pore remains unaffected (Fig. 7a). Such modeled structural rearrangements confirmed earlier postulations that were made in order to explain the sensitivity of SKOR to external K^+ (Johansson *et al.*, 2006): Upon closure, the selectivity filter and larger parts of the permeation pathway must still be accessible from the extracellular space. Pore cavity width analyses further indicated that, also in KAT1, the cytosol-oriented part of the channel undergoes structural rearrangements during gating (Fig. 7b). The degree of changes is, however, less pronounced compared with those in SKOR and the distribution of the alteration shows two interesting differences (Fig. 7c): (i) in a small region at the cytosolic vestibule of the KAT1 pore (around position 5; Fig. 1) the cavity diameter is not changing during the opening process, indicating a static role of this area (Fig. 7c, dashed line) – this finding correlates well with the dominant effect of residue exchanges in this part of the KAT1 channel; (ii) In the central part of the pore (around positions 1–4; Fig. 1) the KAT1 permeation pathway even slightly narrows down during opening while SKOR does not. This finding further supports the conclusion that the central S6 gating domain plays a different role in both channels.

Discussion

The family of voltage-gated K^+ channels in *Arabidopsis* is unusually rich in its functional diversity and gating characteristics, despite the remarkable degree of sequence homogeneity between its family members. Two major subfamilies are characterized, on the one hand, by the gene products KAT1, KAT2, SPIK and AKT1 facilitating inward-rectifying K^+ currents with a predominant sensitivity to voltage, and, on the other, by SKOR and GORK which mediate outward-rectifying K^+ currents that exhibit gating subject to voltage and to extracellular $[K^+]$ (Véry & Sentenac, 2003; Dreyer *et al.*, 2004a; Johansson *et al.*, 2006). Especially intriguing is the unusual sensitivity of SKOR and GORK to $[K^+]_o$ (Gaymard *et al.*, 1998; Ache *et al.*, 2000; Hosy *et al.*, 2003; Johansson *et al.*, 2006) which ensures physiological K^+ efflux, even when $[K^+]_o$ varies over more than three orders of magnitude. A prerequisite for an efficient regulation of ion channel activity by physiological stimuli is the effective conversion of them into changes in the free energy barrier of the gate. For instance, phosphorylation of the Arabidopsis K^+ channel AKT2 reduces the activation energy by *c.* 9 *kT* (Michard *et al.*, 2005a,b). And different occupancies of the pore by K^+ ions modify the activation energy of SKOR in the range of *c.* 3.5–4.0 *kT* (Johansson *et al.*, 2006; and data presented here).

Our previous studies (Johansson *et al.*, 2006) showed voltage- and K^+-dependent gating of SKOR to depend *inter alia* on a core sequence of amino acid residues situated near the centre of the S6 transmembrane α-helix. To investigate the role of the S6 in gating of K_{in} and K_{out} channels, we explored here the functional reciprocity between the six divergent residues in the distal part of the S6 domains of KAT1 and SKOR. We report that mutations in the central and C-terminal parts of S6 influence the gating of both K^+ channels; that, in general, exchange of the corresponding residues between KAT1 and SKOR only yields complementary effects on gating in exceptional cases; that mutations of the central S6 residues in SKOR appear dominant over those at the C-terminus, whereas the reverse is true for KAT1; and that residues KAT1-N297 and SKOR-A325 (position 5) play a special role in KAT1 and SKOR gating. These results highlight the importance of the S6 α-helix for the gating of KAT1 and SKOR, but also underline structural dissimilarities between the two K^+ channels.

The distal parts of the last transmembrane helix S6 are very similar in KAT1 and SKOR. The two channels differ in only six out of 18 amino acid residues. This similarity suggests that both channels inherited their structure from a common

ancestor. The different roles of the S6 region in K_{in} and K_{out} channels would then indicate a divergent evolution of these two channel subclasses. In K_{out} channels, the S6 region is an essential part of the K^+ sensor. Furthermore, it contributes to voltage-dependent gating, indicating that the two processes are closely connected. Notably, both are remarkably fragile in comparison with the robust voltage-gating of the K_{in} channel KAT1. We presume that this difference poses a (possibly insurmountable) obstacle for the transfer of the K^+ sensor from K_{out} to K_{in} channels. Such a synthetic potassium uptake channel, which senses external [K^+] and opens – even under extreme conditions – only when the driving force for K^+ is inwardly directed, could well be of use to improve crop plants for proper growth on K^+-starved soil.

Acknowledgements

We thank Antje Schneider for technical assistance. This work was supported in part by an Erasmus fellowship to PG, by a Heisenberg fellowship of the Deutsche Forschungsgemeinschaft to ID, by a DAAD-fellowship to TS, by a fellowship from CONICYT to WG, by the 'Proyecto Bicentenario de Ciencia y Tecnología (ACT/24)', by the UK Biotechnology and Biological Sciences Research Council (grants 17/C013599, BB/D001528/1 and BB/D500595/1) and by a John Simon Guggenheim Memorial Fellowship to MRB. TS is a member of the International Max-Planck Research School 'Primary Metabolism and Plant Growth' at the University of Potsdam and the Max-Planck Institute of Molecular Plant Physiology.

References

Abagyan R, Totrov M, Kuznetsov D. 1994. Icm – a new method for protein modeling and design – applications to docking and structure prediction from the distorted native conformation. *Journal of Computational Chemistry* **15**: 488–506.

Ache P, Becker D, Ivashikina N, Dietrich P, Roelfsema MR, Hedrich R. 2000. GORK, a delayed outward rectifier expressed in guard cells of *Arabidopsis thaliana*, is a K^+-selective, K^+-sensing ion channel. *FEBS Letters* **486**: 93–98.

Aqvist J, Luzhkov V. 2000. Ion permeation mechanism of the potassium channel. *Nature* **404**: 881–884.

Blatt MR, Garcia-Mata C, Sokolovski S. 2007. Membrane transport and Ca2+ oscillations in guard cells. In: Mancuso S, Shabala SN, eds. *Rhythms in plants*. Heidelberg, Germany: Springer, 115–134.

Blatt MR, Gradmann D. 1997. K^+-sensitive gating of the K^+ outward rectifier in *Vicia* guard cells. *The Journal of Membrane Biology* **158**: 241–256.

Cao Y, Crawford NM, Schroeder JI. 1995. Amino terminus and the first four membrane-spanning segments of the Arabidopsis K^+ channel KAT1 confer inward-rectification property of plant-animal chimeric channels. *The Journal of Biological Chemistry* **270**: 17697–17701.

Dreyer I, Mueller-Roeber B, Köhler B. 2004a. Voltage-gated ion channels. In: Blatt MR, ed. *Membrane transport in plants*. Oxford, UK: Blackwell Publishing, 150–192.

Dreyer I, Poree F, Schneider A, Mittelstädt J, Bertl A, Sentenac H, Thibaud JB, Mueller-Roeber B. 2004b. Assembly of plant *Shaker*-like Kout channels requires two distinct sites of the channel alpha-subunit. *Biophysical Journal* **87**: 858–872.

Essmann U, Perera L, Berkowitz ML, Darden T, Lee H, Pedersen LG. 1995. A smooth particle mesh ewald method. *Journal of Chemical Physics* **103**: 8577–8593.

Gaymard F, Pilot G, Lacombe B, Bouchez D, Bruneau D, Boucherez J, Michaux-Ferriere N, Thibaud JB, Sentenac H. 1998. Identification and disruption of a plant shaker-like outward channel involved in K^+ release into the xylem sap. *Cell* **94**: 647–655.

Hosy E, Vavasseur A, Mouline K, Dreyer I, Gaymard F, Poree F, Boucherez J, Lebaudy A, Bouchez D, Very AA *et al.* 2003. The *Arabidopsis* outward K^+ channel GORK is involved in regulation of stomatal movements and plant transpiration. *Proceedings of the National Academy of Sciences, USA* **100**: 5549–5554.

Johansson I, Wulfetange K, Poree F, Michard E, Gajdanowicz P, Lacombe B, Sentenac H, Thibaud JB, Mueller-Roeber B, Blatt MR *et al.* 2006. External K modulates the activity of the Arabidopsis potassium channel SKOR via an unusual mechanism. *Plant Journal* **46**: 269–281.

Jorgensen WL, Chandrasekhar J, Madura JD, Impey RW, Klein ML. 1983. Comparison of simple potential functions for simulating liquid water. *Journal of Chemical Physics* **79**: 926–935.

Laskowski RA, Macarthur MW, Moss DS, Thornton JM. 1993. Procheck – a program to check the stereochemical quality of protein structures. *Journal of Applied Crystallography* **26**: 283–291.

Long SB, Campbell EB, MacKinnon R. 2005. Crystal structure of a mammalian voltage-dependent *Shaker* family K^+-channel. *Science* **309**: 897–903.

Marquardt DW. 1963. An algorithm for least squares estimation of nonlinear parameters. *Journal of the Society of Industrial and Applied Mathematics* **11**: 431–441.

Mashl RJ, Jakobsson E. 2008. End-point targeted molecular dynamics: large-scale conformational changes in potassium channels. *Biophysical Journal* **94**: 4307–4319.

Michard E, Dreyer I, Lacombe B, Sentenac H, Thibaud JB. 2005a. Inward rectification of the AKT2 channel abolished by voltage-dependent phosphorylation. *Plant Journal* **44**: 783–797.

Michard E, Lacombe B, Poree F, Mueller-Roeber B, Sentenac H, Thibaud JB, Dreyer I. 2005b. A unique voltage sensor sensitizes the potassium channel AKT2 to phosphoregulation. *The Journal of General Physiology* **126**: 605–617.

Naso A, Montisci R, Gambale F, Picco C. 2006. Stoichiometry studies reveal functional properties of KDC1 in plant shaker potassium channels. *Biophysical Journal* **91**: 3673–3683.

Pardo LA, Heinemann SH, Terlau H, Ludewig U, Lorra C, Pongs O, Stuhmer W. 1992. Extracellular K+ specifically modulates a rat brain K+ channel. *Proceedings of the National Academy of Sciences, USA* **89**: 2466–2470.

Pathak MM, Yarov-Yarovoy V, Agarwal G, Roux B, Barth P, Kohout S, Tombola F, Isacoff EY. 2007. Closing in on the resting state of the Shaker K(+) channel. *Neuron* **56**: 124–140.

Phillips JC, Braun R, Wang W, Gumbart J, Tajkhorshid E, Villa E, Chipot C, Skeel RD, Kale L, Schulten K. 2005. Scalable molecular dynamics with NAMD. *Journal of Computational Chemistry* **26**: 1781–1802.

Pilot G, Pratelli R, Gaymard F, Meyer Y, Sentenac H. 2003. Five-group distribution of the *Shaker*-like K^+ channel family in higher plants. *Journal of Molecular Evolution* **56**: 418–434.

Poree F, Wulfetange K, Naso A, Carpaneto A, Roller A, Natura G, Bertl A, Sentenac H, Thibaud JB, Dreyer I. 2005. Plant Kin and Kout channels: approaching the trait of opposite rectification by analyzing more than 250 KAT1-SKOR chimeras. *Biochemical and Biophysical Research Communications* **332**: 465–473.

Sanguinetti MC, Jiang C, Curran ME, Keating MT. 1995. A mechanistic link between an inherited and an acquired cardiac arrhythmia: HERG encodes the IKr potassium channel. *Cell* **81**: 299–307.

Smart OS, Neduvelil JG, Wang X, Wallace BA, Sansom MS. 1996. HOLE: a program for the analysis of the pore dimensions of ion channel structural models. *Journal of Molecular Graphics* **14**: 354–60, 376.

Véry AA, Sentenac H. 2003. Molecular mechanisms and regulation of K^+ transport in higher plants. *Annual Review of Plant Biology* **54**: 575–603.

Yarov-Yarovoy V, Baker D, Catterall WA. 2006a. Voltage sensor conformations in the open and closed states in ROSETTA structural models of K(+) channels. *Proceedings of the National Academy of Sciences, USA* **103**: 7292–7297.

Yarov-Yarovoy V, Schonbrun J, Baker D. 2006b. Multipass membrane protein structure prediction using Rosetta. *Proteins* **62**: 1010–1025.

Zhou Y, Morais-Cabral JH, Kaufman A, MacKinnon R. 2001. Chemistry of ion coordination and hydration revealed by a K^+ channel-Fab complex at 2.0 A resolution. *Nature* **414**: 43–48.

Supporting Information

Additional supporting information may be found in the online version of this article.

Fig. S1 Single mutations in the center of the S6 domain can alter the gating properties of KAT1.

Please note: Wiley–Blackwell are not responsible for the content or functionality of any supporting information supplied by the authors. Any queries (other than missing material) should be directed to the *New Phytologist* Central Office.